Article

Single-Crystal-to-Single-Crystal Transformation and Catalytic Properties of New Hybrid Perhalidometallates

Ali Rayes [1,*], Stephany Zárate-Roldán [2,3], Irene Ara [3], Manel Moncer [1,2], Necmi Dege [4], M. Concepción Gimeno [3], Brahim Ayed [5] and Raquel P. Herrera [2,*]

[1] Laboratoire de Recherche, Catalyse et Matériaux Pour l'Environnement et les Procédés, LRCMEP, (LR19ES08), Faculté des Sciences de Gabès, Campus Universitaire, 6072 Gabès, Tunisia; moncermanel123@gmail.com
[2] Laboratorio de Organocatálisis Asimétrica, Departamento de Química Orgánica, Instituto de Síntesis Química y Catálisis Homogénea (ISQCH), CSIC-Universidad de Zaragoza, C/Pedro Cerbuna 12, 50009 Zaragoza, Spain; szarate.roldan@gmail.com
[3] Departamento de Química Inorgánica, Instituto de Síntesis Química y Catálisis Homogénea (ISQCH), CSIC-Universidad de Zaragoza, C/Pedro Cerbuna 12, 50009 Zaragoza, Spain; xray@unizar.es (I.A.); gimeno@unizar.es (M.C.G.)
[4] Department of Physics, Ondokuz Mayıs University, Samsun 55270, Turkey; necmid@omu.edu.tr
[5] Laboratoire de Physico-Chime des Matériaux, Faculté des Sciences de Monastir, Université Monastir, 5050 Monastir, Tunisia; ayedbrahim@yahoo.com
* Correspondence: ali.rayes@fsb.rnu.tn (A.R.); raquelph@unizar.es (R.P.H.); Tel.: +34-976761190 (R.P.H.)

Abstract: Two new organic–inorganic salts of perhalidometallates with protonated organic amine cations have been synthesized and characterized by X-ray diffraction and thermal analysis. (CHBMAH$_2$)ZnBr$_4$·3/2H$_2$O **1** and (CHBMAH$_2$)ZnCl$_4$ **4** [(CHBMAH$_2$)$^{2+}$: 1,3-cyclohexanebis(methylammonium)] were obtained in single-crystal form. The crystal packing in all of the obtained compounds is governed by the formation of various non-covalent intermolecular forces between tetrahalidometallate anions and organic cations, assisted by water molecules in the hydrates. Hirshfeld surface analysis denotes that the most important contributions to the crystal packing are X···H/H···X (X: Cl, Br, I) and H···H interactions. Interestingly, the compound 1,3-cyclohexanebis(methylammonium)tetrachloridozincate (II) dihydrate, (CHBMAH$_2$)ZnCl$_4$·2H$_2$O **2**, undergoes thermally-triggered single-crystal-to-single-crystal (SCSC) transformation upon dehydration to produce a supramolecular solid compound, 1,3-cyclohexanebis(methylammonium) tetrachloridozincate (II), (CHBMAH$_2$)ZnCl$_4$ **4**. The SCSC transformation causes changes in the lattice parameters and a structural rearrangement. Furthermore, the catalytic properties of (CHBMAH$_2$)ZnCl$_4$·2H$_2$O **2** and (CHBMAH$_2$)CdI$_4$·2H$_2$O **3** have been explored in the acetalization process using various uncommon alcohols, beyond methanol or ethanol, for the first time in the literature, with outstanding results, and opening the door to the formation of alternative acetals.

Keywords: perhalidometallates; X-ray crystal structure; thermal analysis; Hirshfeld surface analysis; catalysis; acetalization

1. Introduction

The possibility of producing novel functional materials with important properties gives a strong stimulus for the research of organic–inorganic hybrid compounds. These materials have attracted much attention, not only for their structural variety, but also for their possible uses as active materials in many applications, ranging from catalysis [1–4], electronics (as organic-inorganic emitting diodes, thin-film transistors, among others), and high-density optical data storage [5,6], to therapeutic chemistry [7–9], passing by photovoltaic instruments. Recently, in 2012, organic–inorganic halide perovskite materials have been introduced in solar cells as interesting alternatives to conventional silicon in terms of cost and efficiency [10–12].

Within the organic–inorganic hybrid materials, perhalidometallates of protonated amines constitute a large family of materials, showing in some cases non-centrosymmetric structures, which are expected to have interesting properties, such as piezoelectricity, ferroelectricity, ferroelasticity, pyroelectricity [13–17], and even uses as catalysts [18,19]. In this case, various non-covalent weak bonds, such as hydrogen bonding and Coulombic and van der Waals interactions, govern the crystal packing of these materials.

On the other hand, a small number of hybrid materials undergo a whole transformation process, in which the single-crystal integrity and the long-range structural order are maintained in a single-crystal-to-single-crystal (SCSC) transformation [20–22], which represents an exceptional phenomenon in materials science. Sometimes, SCSC transformation is accompanied by a rearrangement of the network of intermolecular contacts that stabilizes the crystal packing, which frequently results in noticeable changes in the global structural network. In other cases, independently of any composition variation (removal of guest solvent molecules, exchange of ions, and variation in oxidation states of component atom), the architecture of the rugged frameworks remains intact across the SCSC transformation process. In recent years, there have been many important publications in which these subjects were studied. For example, Roques, Sutter, and co-workers (2011) have described a porous supramolecular zirconium oxalate hydrate $[\{(H_2\text{-}L1)_2Zr(C_2O_4)_4\}\cdot 2H_2O]$ (with L1: *p*-bis(imidazol-1-yl)benzene) [23] which undergoes reversible SCSC dehydration. The dehydrated form crystallizes in the same group with the same lattice parameters. In contrast, Kinzhybalo and co-workers (2018) have reported a compound tetra-*n*-butylammonium hypodiphosphate hydrate [24] in which water is removed from the crystal upon heating, accompanied by a reorganization of the ions present in the crystal.

We report the chemical preparation and crystal structure of a new hybrid perhalidometallate $(CHBMAH_2)ZnBr_4\cdot 3/2H_2O$ **1**, obtained in the presence of diprotonated 1,3-cyclohexanebis(methylammonium) (abbreviated: $(CHBMAH_2)^{2+}$). Additionally, the relationship with other similar structures recently reported by Rayes et al., namely $(CHBMAH_2)ZnCl_4\cdot 2H_2O$ **2** and $(CHBMAH_2)CdI_4\cdot 2H_2O$ **3** [25], is discussed in the present work. Interestingly, the compound $(CHBMAH_2)ZnCl_4$ **4** was obtained as a result of a solid state dehydration process of **2** by heating it up to 140 °C. Hence, it constitutes a new example of the uncommon single-crystal-to-single-crystal (SCSC) transition and has also been studied by single-crystal X-ray diffraction. Furthermore, the catalytic activities of 2 and 3 are explored in a model and basic reaction, the acetalization of aldehydes to give acetals, to find a plausible application of our structures.

2. Results

We initiated the study with the characterization of the chemical and physical properties of compounds **1** and **4**.

2.1. Structure Description of $(CHBMAH_2)ZnBr_4\cdot 3/2H_2O$ **1**

Crystal structures for compounds **1** and **4** have been determined by single-crystal XRD. Crystallographic data and structure-refinement parameters for compounds **1** and **4** are summarized in Table 1.

The new compound $(CHBMAH_2)ZnBr_4\cdot 3/2H_2O$ **1** crystallizes in the orthorhombic system with a non-centrosymmetric space group $P2_12_12$ and a Flack parameter of 0.014(6), indicating that the absolute structure given by the structure refinement is correct. In addition, the asymmetric part of the unit cell contains diprotonated 1,3-cyclohexanebis(methylammonium) $(CHBMAH_2)^{2+}$, the tetrabromidozincate (II) anion $(ZnBr_4)^{2-}$, and water molecules (Figure 1).

**Table 1.** Crystallographic data and structural refinement parameters for compounds **1** and **4**.

	1	**4**
Chemical formula	$(CHBMAH_2)ZnBr_4 \cdot 3/2H_2O$	$(CHBMAH_2)ZnCl_4$
Formula weight (g mol^{-1})	556.29	351.43
Temperature (K)	296	296
Crystal system	Orthorhombic	Monoclinic
Space group	$P2_12_12$	$P2_1/c$
a (Å)	12.5741(8)	7.2772(7)
b (Å)	21.0211(14)	9.8130(9)
c (Å)	6.7709(4)	22.009(2)
α (°)	90	90
β (°)	90	96.1760(10)
γ (°)	90	90
Volume (Å^3)	1789.7(2)	1562.6(3)
Z	4	4
Density (g·cm^{-3})	2.065	1.494
Absorption coefficient (mm^{-1})	10.293	2.230
F(000)	1068	720
Theta range (°)	2.255–25.155	2.274–23.541
Reflections measured	15,931	13,805
Independent reflections	5186	4500
Reflections included [I > 2σ(I)]	3785	2761
R(int)	0.036	0.04
Restraints/parameters	0/162	0/174
Goodness-of-fit	0.947	1.063
Refinement on	F^2	F^2
Final R indices	R = 0.0326	R = 0.0711
-	R_w = 0.0689	R_w = 0.2078
$\Delta\rho_{max}$, $\Delta\rho_{min}$ (e Å^{-3})	−0.595, 0.914	−0.601, 1.593
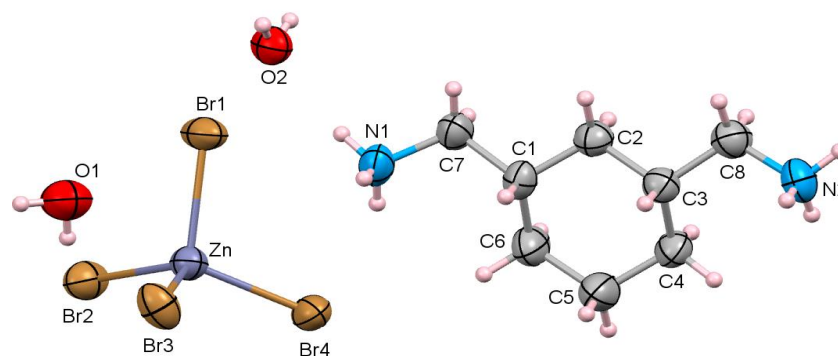
Figure 1. The asymmetric unit of $(CHBMAH_2)ZnBr_4 \cdot 3/2H_2O$ **1** (50% probability displacement ellipsoids).

The cation and one water molecule occupy general positions, while the second water molecule is located on a two-fold rotation axis. Non-covalent forces maintain the cohesion and stability of the crystalline network. These interactions comprehend hydrogen bonding, Coulomb interactions, and van der Waals forces. Four bromine atoms surround the central zinc atom in a slightly distorted tetrahedral geometry. The Zn-Br bond lengths vary from 2.3925(9) to 2.4357(8) Å, and the Br-Zn-Br bond angles range from 104.43(3)° to 113.75(3)°, and are similar to those observed in other compounds containing the same anion [26–29] (Table S1). This significant difference in these geometric parameters can be ascribed mainly to H-bonds, making the $ZnBr_4^{2-}$ tetrahedron softly distorted. This distortion is determined by the calculation of the geometry index τ_4 [30] for four-coordinated species, which quantifies the degree of distortion of the coordination polyhedron from ideal tetrahedral ($\tau_4 = 1$) to perfectly square planar ($\tau_4 = 0$). This τ_4 parameter is defined as the difference between 360 and the sum of the two largest angles divided by 141. In the present case, the tetracoordinated Zn atom has a slightly distorted tetrahedral conformation, with a τ_4 index of 0.952.

This value confirms the involvement of the Br atoms in a complex system of N–H···Br and O–H···Br H-bonds at the origin of the slight distortion of $ZnBr_4^{2-}$ from the ideal tetrahedral geometry. In this compound, each $ZnBr_4^{2-}$ unit connects to four water molecules through O–H···Br H-bonds. The resulting 3-D H-bonded anionic framework $\{(ZnBr_4\text{-OW})^{2-}\}_n$ contains large channels (section dimensions of 15.438 Å × 7.482 Å) running along [100] the crystallographic direction. These channels are filled by the diprotonated $(CHBMAH_2)^{2+}$ cations to maximize the Coulombic forces and are linked to the anionic framework through N–H···OW and N–H···Br H-bonds (Figure 2). H-bond lengths and angles of compound **1** are reported in Table 2.
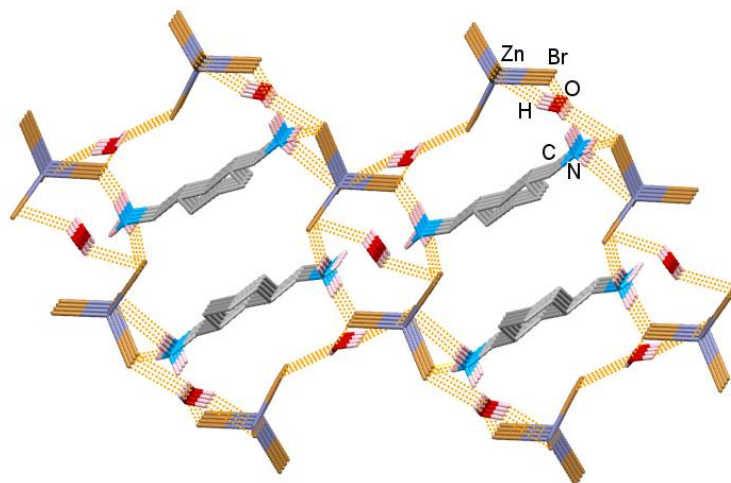
Figure 2. Partial packing diagram of $(CHBMAH_2)ZnBr_4\cdot3/2H_2O$ **1** viewed along the **c** axis and showing the H-bonding network (dashed lines).

Table 2. H-bond lengths (Å) and angles (°) in $(CBMH_2)ZnBr_4\cdot3/2H_2O$ **1**.

D–H···A	D–H	H···A	D···X	D–H···X
N1-H1B···Br2	0.89	2.725 (1)	3.391 (5)	164.4 (3)
N1-H1C···Br4	0.89	2.826 (1)	3.459 (5)	129.3 (3)
N2-H2C···Br3	0.89	2.492 (1)	3.366 (5)	167.1 (3)
N2-H2E···Br1	0.89	2.641 (1)	3.351 (5)	137.4 (3)
C2-H2A···Br3	0.97	3.022 (1)	3.788 (6)	136.7 (4)
O1-H2W1-Br4	0.85	2.94 (9)	3.461 (6)	121 (7)
O1-H1W1-Br1	0.85	2.60 (1)	3.290 (7)	147 (9)
O2-H1W2-Br2	0.73 (8)	2.92 (8)	3.579 (6)	150 (7)

2.2. Structure Discussion

The geometry examination of the organic cation $(CHBMAH_2)^{2+}$ indicates that the cyclohexane ring adopts a chair conformation in compound **1**. This conformation is the most stable arrangement of the carbon atoms in the C6-ring. It is important to note that the reaction of a mixture of *cis* and *trans* isomers of CHBMA with a suitable proportion of anhydrous zinc bromide and hydrobromic acid results in pure *cis* isomers in the synthesized crystal. This selectivity for the *cis* configuration in **1** has also been observed in the compounds $(CHBMAH_2)ZnCl_4\cdot2H_2O$ **2** and $(CHBMAH_2)CdI_4\cdot2H_2O$ **3** [25]. In contrast, in other compounds containing the same organic cation $(CHBMAH_2)^{2+}$, such as $(CHBMAH_2)Zn_{2.1}Co_{0.9}(HPO_3)_4$ [31] and $(CHBMAH_2)(NO_3)_2$ [32], the *trans* configuration has also been found. Interestingly, this crystallization process may be used as a possible technique for the separation and recognition of *cis* and *trans* isomers of CHBMA.

On the structural side, for the same *cis* configuration observed in **1**, **2** and **3**, the two terminal ammonium groups in the organic moiety show two possible orientations, upward for **3** and downward for **1** and **2** (Figure 3).
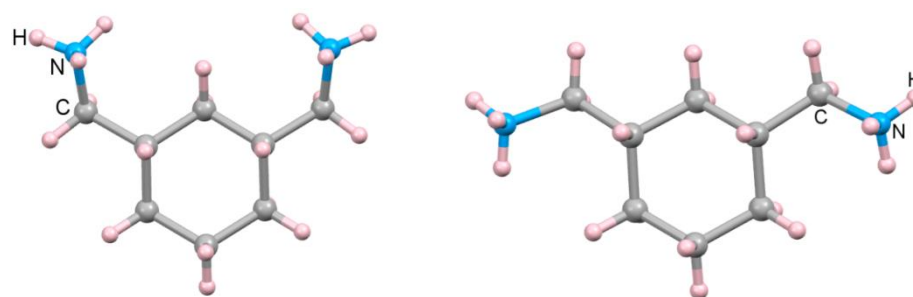
Figure 3. The two methylammonium groups exist in the *cis* configuration with upward orientation (**left**) and downward orientation (**right**).

This difference in orientation is reflected in the different connectivity of the ammonium groups in the organic moiety on the anionic framework and, therefore, in an H-bonded network with different dimensionality. Consequently, the interconnection of organic cations and anionic frameworks is achieved in a 3-D H-bonded network in **1** (Figure 2) and **3** (Figure 4a), while it is performed in a 2-D H-bonded network in **2** (Figure 4b).
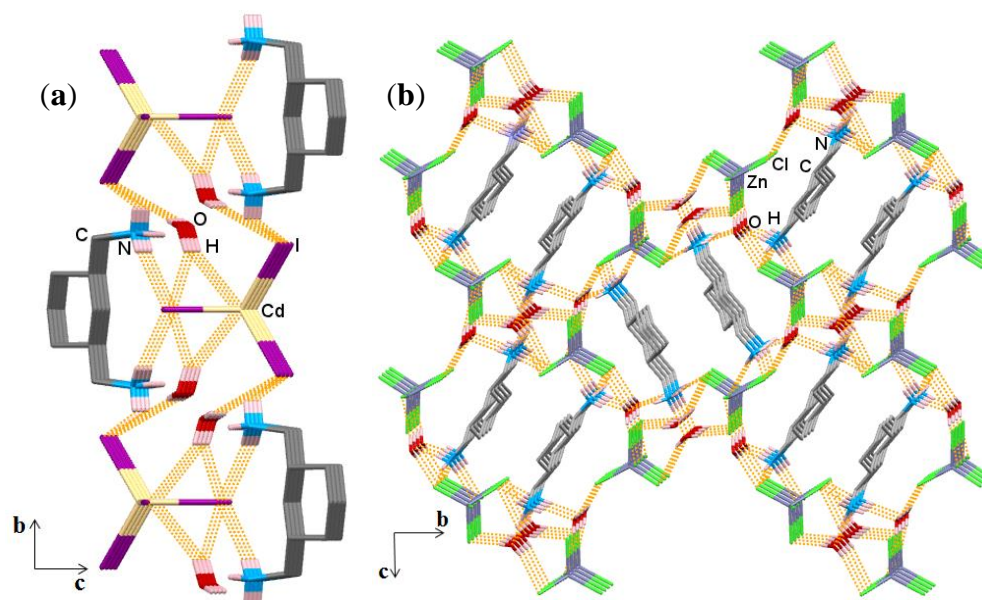

Figure 4. Depending on the orientation of the ammonium groups of the $(CHBMAH_2)^{2+}$, two assembling patterns have been observed, (**a**) two-dimensional (2-D) in **3** (upward orientation) and (**b**) three-dimensional (3-D) in **2** (downward orientation) H-bonded networks.

2.3. Thermal Analyses (DTA/TGA)

In order to examine the thermal behavior of the crystalline supramolecular species $(CHBMAH_2)ZnBr_4 \cdot 3/2H_2O$ **1**, two curves corresponding to the differential thermal/ thermogravimetric analyses (DTA/TGA) were carried out from 20 to 600 °C (Figure 5).

The TGA indicates a first weight loss upon heating to about 120 °C, which corresponds to the complete release of the H_2O molecules. After solvent release, the dehydrated phase remains stable up to the melting point at 182.5 °C. Signs of chemical decomposition of the framework are observed above 290 °C. It is important to note that comparable thermal behaviors have been observed for the two materials $(CHBMAH_2)ZnCl_4 \cdot 2H_2O$ **2** and $(CHBMAH_2)CdI_4 \cdot 2H_2O$ **3** [25].
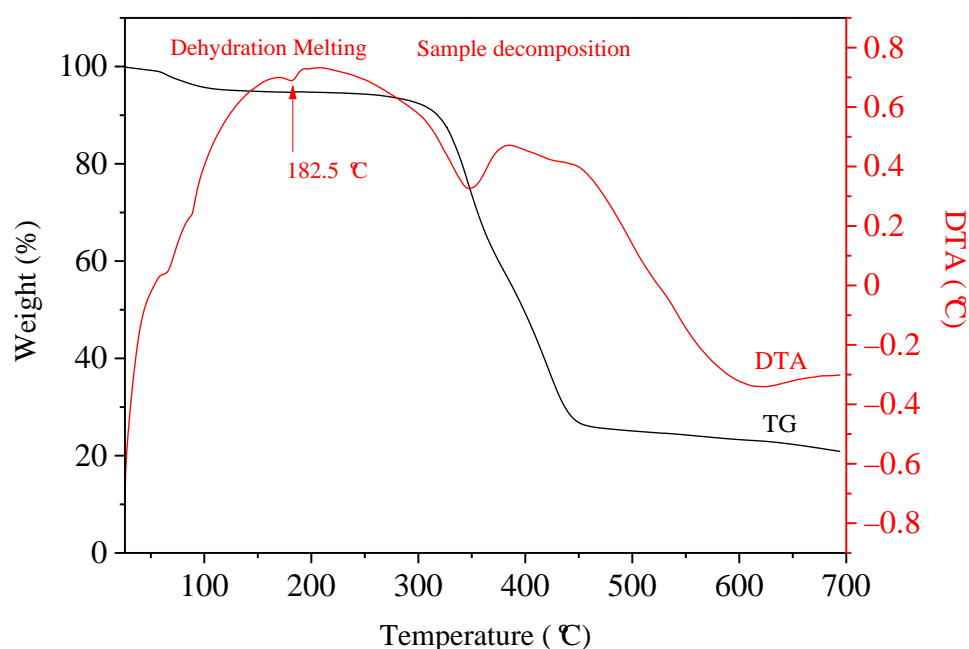
Figure 5. Differential thermal/thermogravimetric analyses of (CHBMAH$_2$)ZnBr$_4$·3/2H$_2$O **1**.

2.4. Single-Crystal-to-Single-Crystal (SCSC) Transformation. Crystal Structure of (CHBMAH$_2$)ZnCl$_4$ **4** and Comparison with That of **2**

Intending to obtain structural information on the crystalline phases formed after dehydration, we heated a few single crystals of each compound **1**–**3** in a muffle furnace to about 140 °C for 45 min. After cooling to room temperature, the single-crystal **2** appeared intact and transparent, while the other two, **1** and **3**, became opaque. Therefore, a single-crystal XRD analysis at 298 K was envisioned for these three materials. Upon heating, **1** and **3** lost the single-crystal integrity, resulting in a crystalline powder, but **2** underwent a single-crystal-to-single-crystal phase transition. Diffraction data collected at 298 K for the new single-crystal phase **4** allowed the resolution and refinement of the crystal structure.

The single-crystal X-ray structure analysis of **4** reveals that water molecules trapped in the structure of **2** are evacuated from the network after heat treatment.

To our knowledge, **2** is the first example in perhalidometallate hybrid chemistry of a solid-state transition for which the structures of the initial and final crystalline states are investigated by single-crystal XRD.

The XRD study shows that the dehydrated form **4** crystallizes in the same space group P2$_1$/c as the hydrated form **2,** but with different cell parameters. The asymmetric part of the unit cell, depicted in Figure 6a, comprises an isolated tetrachlorozincate(II) anion (ZnCl$_4$)$^{2-}$ and a diprotonated 1,3-cyclohexanebis(methylamine) (CHBMAH$_2$)$^{2+}$ cation. The latter is disordered, over two possible ring positions with the same occupancy (Figure 6b).

The structure of **4** consists of a 3-D framework composed of (CHBMAH$_2$)$^{2+}$ cations and the tetrachloridozincate(II) anions connected by N–H···Cl hydrogen bonds and additionally stabilized by Coulombic interactions. In the anion, the Zn^{II} atom is coordinated by four Cl atoms in a slightly distorted tetrahedral geometry (τ_4 = 0.95), with Zn–Cl bond lengths ranging from 2.262 (2) Å to 2.282 (18) Å, and the Cl–Zn–Cl bond angles varying between 106.33 (7)° and 114.22 (8)° (Table S2). These geometry parameters are in the same magnitude as those observed in homologous compounds containing isolated anions [ZnCl$_4$]$^{2-}$ [33–37].

The cyclohexane ring shows a chair conformation and has been modelled as disordered over two positions at half occupancy. C2 and C5 belong to both rings and have been refined at full occupancy. Therefore, one of the rings is formed by C1, C2, C3, C4, C5 and C6 and the other ring is formed by C1′, C2, C3′, C4′ C5 and C6′ (Figure 7 below). The disordered organic cation (CHBMAH$_2$)$^{2+}$ presents a *cis* configuration in which the two terminal

ammonium groups are pointing downward, thus promoting a 3-D H-bond network with the chlorine atoms of $ZnCl_4^{2-}$ anions.
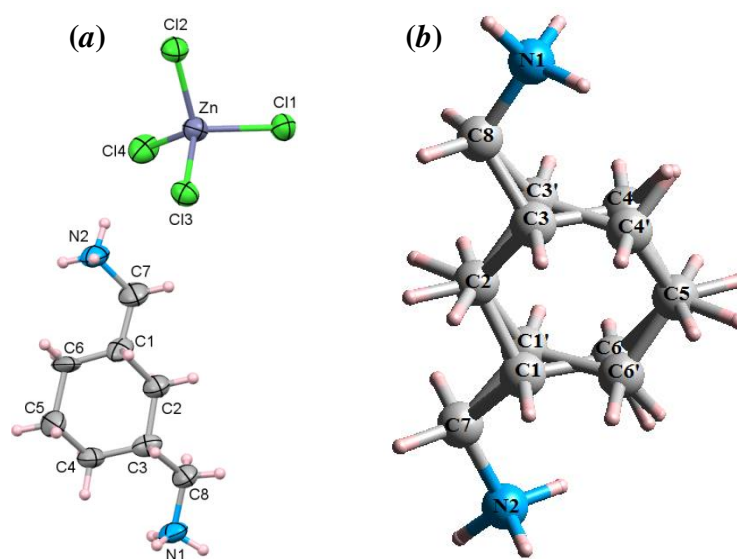
Figure 6. The asymmetric unit of the $(CHBMAH_2)ZnCl_4$ **4** (50% probability displacement ellipsoids) (**a**), the cyclohexane ring in **4** is disordered in two orientations (**b**).

Examination of the C–C, C–N distances and C–C–C, C–C–N angles in the $(CHBMAH_2)^{2+}$ dication shows that they are comparable to those found in other works [4,25] (Table S2).

The dehydration process in **2** is accompanied by the breakage of medium-strength O–H···Cl and N–H···O H-bonds between H_2O and the ions ($ZnCl_4^{2-}$, $CHBMAH_2^{2+}$) inside the initial (parent) single crystal, and a reorganization of the ions within the final dehydrated form. This transformation results in an approach between the cationic part and the anionic part and, therefore, in a new organization based on a 3-D H-bond network showing channels propagating in the crystallographic direction [100] (Table 3, Figure 7). This crystalline structure has an important topology to obtain a porous supramolecular solid.

Table 3. H-bond geometry (Å, °) of $(CHBMAH_2)ZnCl_4$, **4**.

D–H···A	D–H	H···A	D···X	D–H···X
N1–H1A···Cl3	0.89	2.493 (2)	3.260 (5)	144.8 (3)
N1–H1C···Cl3	0.89	2.772 (2)	3.435 (6)	132.3 (3)
N1–H1C···Cl1	0.89	2.670 (2)	3.416 (6)	142.1 (3)
N1–H12···Cl2	0.89	2.444 (2)	3.327 (6)	171.4 (3)
N2–H2A···Cl4	0.89	2.634 (2)	3.468 (7)	156.5 (4)
N2–H2B···Cl2	0.89	2.349 (2)	3.180 (6)	155.5 (4)
N2–H2C···Cl1	0.89	2.383 (2)	3.260 (6)	168.7 (4)
C8–H8A···Cl3	0.97	2.864 (2)	3.583 (8)	131.7 (4)

The crystal structure of the hydrated compound **2** did not show any channels from which water molecules would output (Figure 7 above), in contrast to the proposal put forth by Perrier & Byrn (1982) [38]. After dehydration, our results confirm the genesis of such channels. This leads us to establish with certainty that the escape of water from **2** shifts significantly the arrangement of the ions $ZnCl_4^{2-}$ and $(CHBMAH_2)^{2+}$ in the crystal.

Our results also show that hydrogen bonds N–H···Cl in the anhydrous crystal are slightly weaker than in the hydrated crystal **2**. However, Coulombic interactions in the dehydrated crystal **4** are stronger than in **2** because of the elimination of water which acts as a screen between the anions $ZnCl_4^{2-}$ and the cations $(CHBMAH_2)^{2+}$.
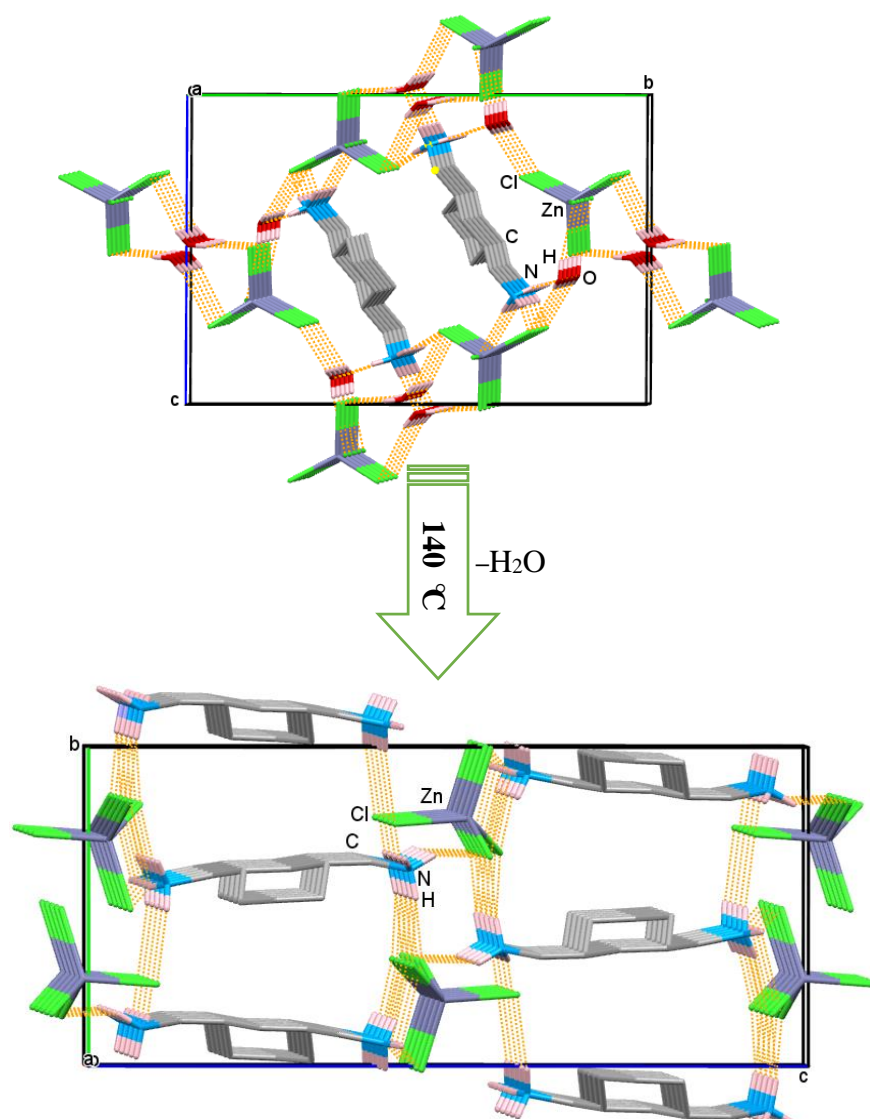
Figure 7. Single-crystal-to-single-crystal irreversible phase transition for compound (CHBMAH$_2$)ZnCl$_4$·2H$_2$O **2** (**above**) to compound (CHBMAH$_2$)ZnCl$_4$ **4** (**below**). Cell axes: **a**, **b**, **c**.

2.5. Hirshfeld Surface Analysis

Three-dimensional Hirshfeld surface analysis was used to understand the nature of intermolecular interactions responsible for the crystal packing. Moreover, the 2-D fingerprint plots quantitatively detected the contribution of those interactions in the crystal structure.

Hirshfeld surfaces mapped over d$_{norm}$ (normalized distance) are shown in Figures S1 and S2, respectively for compounds **1** and **4**. d$_{norm}$ combines both d_e (external distance) and d_i (internal distance), and each distance is normalized by the van der Waals radius for the particular atoms involved in the close contact to the surface. The red spots denote strong H-bonds and interatomic contacts. These correspond to the near-type H···O and H···X (X: Br, Cl, I) contacts resulting from N–H···O and N–H···X hydrogen bonds.

The intermolecular interactions involved in **1** and **4** present as distinct spikes in the two-dimensional fingerprint plots, with the d$_{norm}$ view of individual interactions introduced in Figures S1 and S2.

The percentage contribution of different intermolecular interactions in **1** and **4** are obtained from two-dimensional fingerprint plots and are presented as a chart in Table 4.

Table 4. Percentage contributions of interatomic contacts to the Hirshfeld surface for compounds **1** and **4**.

(CHBMAH$_2$)ZnBr$_4$·3/2H$_2$O, 1		(CHBMAH$_2$)ZnCl$_4$, 4	
Contact	% Contribution	Contact	% Contribution
Br···H/H···Br	53.4	Cl···H/H···Cl	63.4
H···H	35.7	H···H	33.9
O···H/H···O	8.9	Cl···Cl	2.1
Br···Br	0.9	H···Zn/Zn···H	0.4
H···Zn/Zn···H	0.8	Cl···Zn/Zn···Cl	0.3
Br···Zn/Zn···Br	0.3	-	-

According to this chart, the highest interaction contributing to the cohesion of the solid-state structures of **1** and **4** is from M–X···H contacts, followed by H···H van der Waals contacts as deduced from the analysis of decomposed fingerprint plots. The contribution from X···H interactions varies from 53.4% in **1** to 63.4% in **4**. It can be attributed to N–H···X, O–H···X and C–H···X interactions due to the involvement of tetrahalidometallate ions in hydrogen bonding. In the hydrated compound **1**, it is interesting to note that in N–H···O, strong H-bonds are also present, with contributions of 8.9%.

On the other hand, when comparing the fingerprint plots for **2** and **4** [25], the highest difference is regarding the O···H contact, which accounted for 5.5% of the total interactions in **2** but is absent in **4**. This difference is relevant, confirming that compound **2** undergoes a dehydration reaction giving rise to the dehydrated compound **4**. These fingerprint plots are compared in Figure 8.
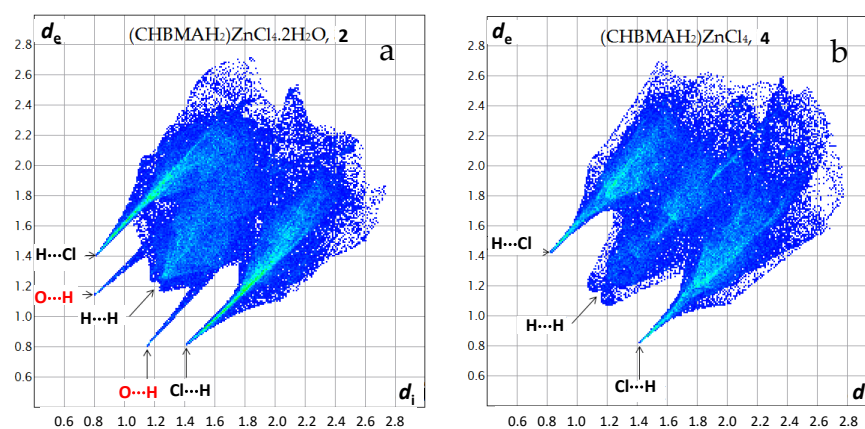
Figure 8. Comparison of fingerprint plots for (**a**) hydrated compound **2** and (**b**) dehydrated compound **4**.

These results agree with the X-ray diffraction analysis of hydrogen bonding interactions and the close packing of tetrahalidometallate anions, water molecules and organic cations.

3. Discussion

After the characterization of these compounds in terms of X-ray studies and Hirshfeld surface and thermal (DTA/TGA) analysis, all of them describing the different properties of these interesting compounds, we decided to go a step further and explore their utility as plausible homogenous catalysts in the acetalization process. For this study, we selected complexes **2** and **3** [25].

The protection of carbonyl groups is one of the most recurrent protocols and powerful tools in organic synthesis for the preparation of cyclic or acyclic acetal intermediates in the synthesis of natural products and important targets [39–42]. Subsequently, they can

also be transformed into a broad spectrum of different functional groups, to be used as intermediates in subsequent processes.

Although this approach has been largely studied for decades due to its relevance and utility, the reported protocols typically require long reaction times and high temperatures. They also afford, in some cases, incomplete reactions with moderate yields, or they are limited to the use of orthoester reagents [43–56]. These are common inconveniences that can potentially limit their utility, but still promote the development of new procedures to overcome such problems.

Despite the plethora of works focused on this carbonyl protection, to the best of our knowledge only scarce examples of Co- [57,58] and Zn-based catalysts [4,18,59,60] have been studied in the literature so far. Interestingly, some of them are pivotal procedures developed by us using simple MeOH as the source of methylation [4,18,60].

The acetalization approach still represents a pivotal challenge since, in many organic reactions or during a multistep synthesis, a carbonyl group could require protection to avoid its reactivity against the attack of different reagents present along the process. Moreover, in these cases, the challenge to overcome this problem could be how to protect this functionality in the presence of a variety of other sensitive functional groups. Although normal protecting groups could involve tedious processes or the use of more expensive orthoesters, we would like to disclose our simple methodology using different accessible but uncommon alcohols, less used in this process until now in the literature.

Therefore, in this spectrum of physico-chemical properties studied with these compounds, we also decided to test the reactivity of these complexes in the acetalization reaction of aldehydes with different alcohols. We went a step further in this study, and although $CH(OMe)_3$ is the most frequently used source of acetalization in the protection of carbonyl compounds, and our previous works were focused on the use of MeOH as the most accessible source, here, we have explored more complex alcohols to provide a higher added value to our methodology and for the progression of this field. Therefore, all developed procedures for the synthesis of non-cyclic acetals are usually limited to dimethyl and diethyl acetals (i.e., the availability of the corresponding orthoesters limits their applicability or the use of MeOH and EtOH).

Based on our previous works, we started screening both catalysts comparatively with preliminary selected conditions (0.1 mmol of aldehyde, 250 μL of alcohol and 5–10 mol% of catalysts) (see the results in Table 5). Interestingly, we have selected a battery of alcohols that have been overlooked or scarcely explored in the literature so far for this reaction. Due to the high number of proofs performed to optimize the best reaction conditions, in Table 5 only the best result for each alcohol is provided.

Although both catalytic structures show the same order of reactivity against the great variety of alcohols tested, it seems that, in general, Cd-based catalyst **3** affords better results. Interestingly, we obtained outstanding conversion values with alcohols that have not been used previously in this protocol, or they have been scarcely explored, allowing the obtainment of new acetal structures. Among the variety of alcohols tested, we decided to continue with 1-pentanol **6e** as a very uncommon source of acetalization. The reaction with alcohol **6e** was also set up in the absence of catalyst **3**, but the process did not work, demonstrating the necessity of our catalytic species in the reaction medium. After this screening of alcohols, and with the best reaction conditions in hand (using 1-pentanol (**6e**) as the source of acetalization and catalyst **3** at 10 mol%), the scope of the reaction was further explored, extending our strategy to different substituted aldehydes, as shown in Figure 9.

Table 5. Comparative reactivity between **2** and **3** using different alcohols as an acetylation source [a].
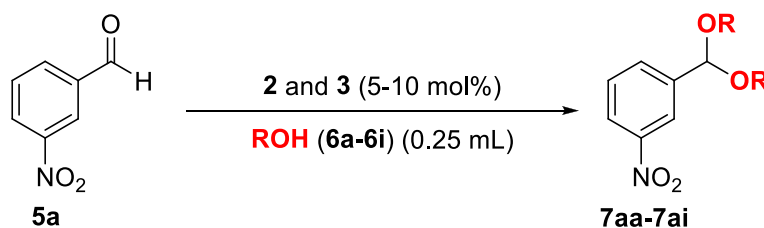
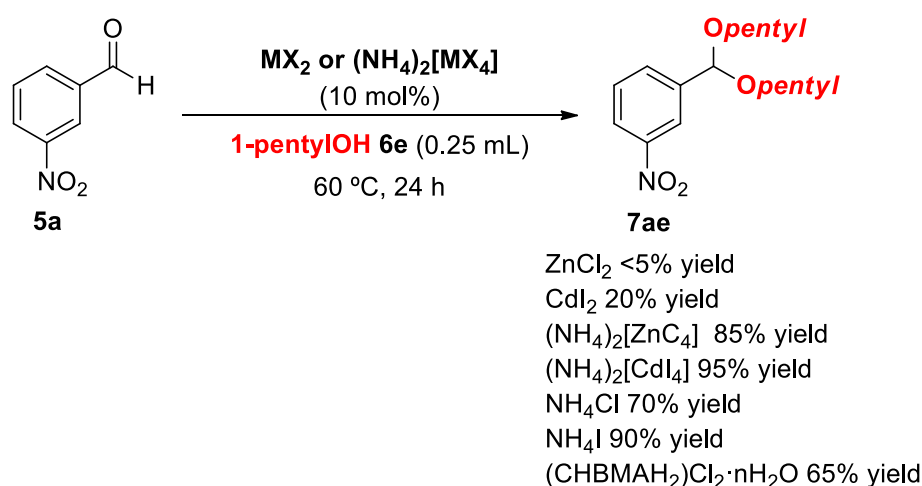| (CHBMAH$_2$)ZnCl$_4$·2H$_2$O, 2				(CHBMAH$_2$)CdI$_4$·2H$_2$O, 3			
Alcohol (6a–6i)	Temp. (°C)	Time (h)	Yield (%)	Alcohol (6a–6i)	Temp. (°C)	Time (h)	Yield (%)
MeOH (**6a**) (10 mol%)	50	24	76	MeOH (**6a**) (10 mol%)	50	24	94
EtOH (**6b**) (5 mol%)	40	24	72	EtOH (**6b**) (5 mol%)	40	24	79
1-PrOH (**6c**) (5 mol%)	60	72	75	1-PrOH (**6c**) (5 mol%)	60	72	76
1-BuOH (**6d**) (5 mol%)	60	72	85	1-BuOH (**6d**) (5 mol%)	60	72	93
1-Pentanol (**6e**) (5 mol%)	60	48	71	1-Pentanol (**6e**) (10 mol%)	60	24	97
1-HexOH (**6f**) (5 mol%)	60	72	69	1-HexOH (**6f**) (5 mol%)	60	72	91
2-Methylbutanol (**6g**) (10 mol%)	60	24	64	2-Methylbutanol (**6g**) (10 mol%)	60	24	83
2-PrOH (**6h**) (10 mol%)	60	24	77	2-PrOH (**6h**) (10 mol%)	50	24	44
1-BnOH (**6i**) (5 mol%)	60	48	52	1-BnOH (**6i**) (5 mol%)	60	48	n.d.

[a] Otherwise indicated: a mixture of aldehyde **5** (0.1 mmol) and catalyst **2** or **3** (5–10 mol%) in 0.25 mL of alcohols **6a–6i**, was stirred at 40–60 °C for the indicated time. After the reaction time, the conversion was calculated by ^{1}H-NMR.
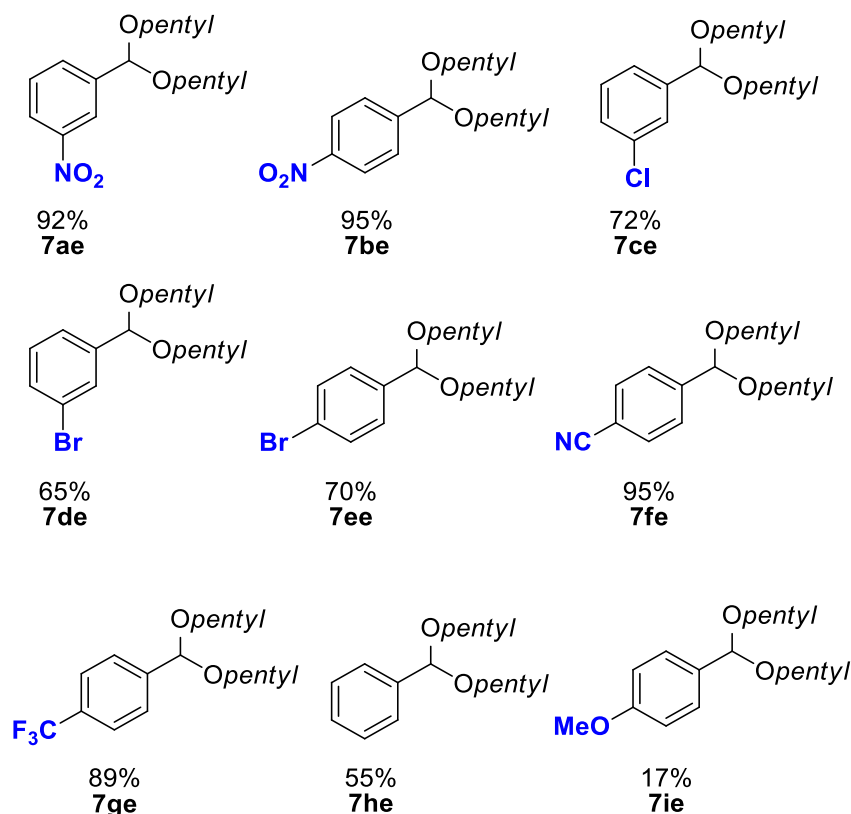
Figure 9. Scope of the reaction. Experimental conditions: a mixture of aldehydes (0.1 mmol) and catalyst (10 mol%) in 0.25 mL of *n*-amyl alcohol **6e** was stirred at 60 °C. After 24 h, the reaction crudes were purified by column chromatography.

As disclosed in Figure 9, the desired acetals **7ae–7ie** were obtained from low to very excellent yields. The developed methodology works better with electron-withdrawing groups in the aromatic ring. Unfortunately, electron-donor groups such as MeO afforded the desired final product **7ie** with lower yield, and benzaldehyde only provided moderate yields (**7he**). This fact can be justified because electron-withdrawing groups in the aromatic ring make the carbonyl group of the aldehyde more electrophilic to receive the first attack of the alcohol as a nucleophile, and opposite occurs with electron-donating groups. The crudes of the reactions are very clean. Interestingly, neither inert nor dry atmosphere or other special conditions were needed to carry out the reactions. Moreover, this is the first time this alcohol has been used as the source of acetalization in this procedure, providing a new acetal structure family.

In order to know the role of the catalytic species, we have performed additional experimental proofs where the contribution of each fragment of the complex has been explored separately. For this purpose, we have used $ZnCl_2$, CdI_2, $(NH_4)_2[ZnCl_4]$, $(NH_4)_2[CdI_4]$, NH_4Cl, NH_4I and $(CHBMAH_2)Cl_2$. All these species were prepared by us, except $ZnCl_2$ and CdI_2, which are commercially available (Scheme 1).

$ZnCl_2$ <5% yield
CdI_2 20% yield
$(NH_4)_2[ZnC_4]$ 85% yield
$(NH_4)_2[CdI_4]$ 95% yield
NH_4Cl 70% yield
NH_4I 90% yield
$(CHBMAH_2)Cl_2 \cdot nH_2O$ 65% yield

Scheme 1. Additional catalytic proofs. After the reaction time, the conversion was calculated by ^{1}H-NMR respect to the aldehyde.

Interesting statements can be concluded with these results. First, zinc chloride and cadmium iodide do not promote the reaction efficiently. In contrast, ammonium salts exhibit much higher activity. In general, slightly better results are obtained with Cd derivatives (CdI_2 vs. $ZnCl_2$ and $(NH_4)_2[CdI_4]$ vs. $(NH_4)_2[ZnCl_4]$), as also observed by us with catalysts **2** and **3** (Table 5), due to the most electropositive properties of Cd against Zn. Comparatively, complex **3** used in our developed procedure seems to provide similar good results to $(NH_4)_2[CdI_4]$. The different results obtained with the ammonium metal halogenates is noteworthy. We cannot discard that the differences in the solubility of these species could also affect their activity, and, consequently, the ammonium moieties may play an important role in these complexes. The use of NH_4Cl and NH_4I also afforded very good results. In contrast, the real cation of our species in **2** and **3**, $(CHBMH_2)Cl_2 \cdot nH_2O$ afforded only 65% yield. Therefore, in our species **2** and **3,** a synergistic effect in the acidity of the system should exist in order to arrive at quantitative yield values as reported in Table 5 and Figure 9, concluding that both parts of the structures are necessary (see the values obtained with $CdI_4(NH_4)_2$ and $ZnCl_4(NH_4)_2$ in comparison with CdI_2 or $ZnCl_2$ and NH_4I or NH_4Cl, respectively). The value obtained with the catalyst $(CHBMAH_2)ZnCl_4 \cdot 2H_2O$ **2** in Table 5 (71%) in comparison with their species separately $ZnCl_2$ (5%) and $(CHBMH_2)Cl_2$ (51%) is also remarkable. A synergistic effect beyond our understanding should be invoked to understand the better yields obtained with both parts of the catalysts. At this point, maybe computational calculations could support a more concrete mechanism.

4. Materials and Methods

All the used chemicals zinc(II) bromide, zinc(II) chloride, cadmium(II) iodide, hydrobromic acid (47%), hydrochloric acid (37%), and 1,3-cyclohexanebis(methylamine), abbreviated CHBMA, were obtained from commercial sources and used without further purification. CHBMA was purchased as a mixture of *cis* and *trans* isomers.

Simultaneous thermogravimetric and differential thermal analysis (TGA-DTA) data were obtained using a TG-DTA 2960 SDT thermal analyzer. The sample (m = 4.40610 mg) was placed in an open alumina crucible and heated, under nitrogen flow N_2, from room temperature to 600 °C with a 10 °C/min heating rate; an empty crucible was used as reference.

Purification of the reaction products was carried out by column chromatography using neutral alumina. Analytical thin layer chromatography was performed on 0.25 mm silica-gel 60-F plates. An ESI and a MicroTof-Q mass analyzer were used for HRMS measurements. ^{1}H NMR spectra were recorded at room temperature on a BRUKER AVANCE II 300 spectrometer (^{1}H, 300 MHz), with chemical shifts (ppm) reported relative to the solvent peaks of the deuterated solvent. CD_3CN was used as the deuterated solvent. Chemical shifts were reported in the δ scale relative to residual CH_3CN (1.94 ppm) for ^{1}H-NMR and to the central line of CD_3CN (1.32 ppm) for ^{13}C-APT NMR.

4.1. Synthesis

4.1.1. Synthesis of (CHBMAH$_2$)ZnBr$_4$·3/2H$_2$O, 1

Crystals of (CHBMAH$_2$)ZnBr$_4$·3/2H$_2$O were obtained at room temperature by the slow evaporation of an aqueous solution containing 1,3-cyclohexyl(methylamine) (CHBMA), ZnBr$_2$ and hydrobromic acid HBr (47%) in a 1:1:2 molar ratio. The reaction can be schematically written as:

$$HBMA + (Zn^{2+}, 2Br^-) + 2(H_3O^+, Br^-) \rightarrow (CHBMAH_2)ZnBr_4 \cdot 3/2H_2O + 0.5H_2O$$
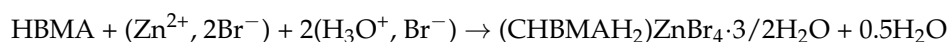
The reaction mixture was stirred for 20 min until complete dissolution occurred. After slow evaporation of the solution at room temperature over a period of 7 days, air stable colorless crystals of **1** suitable for X-ray diffraction were selected (yield ~ 55%).

4.1.2. Synthesis of (CHBMAH$_2$)ZnCl$_4$, 4

The new compound (CHBMAH$_2$)ZnCl$_4$ **4** was obtained by heating the hydrated sample (CHBMAH$_2$)ZnCl$_4$·2H$_2$O **2** [25] at a temperature of about 140 °C for 45 min and then cooling to room temperature.

4.2. Crystal Structures Determination and Refinement

Crystal structures for compounds **1** and **4** have been determined by single-crystal XRD [61]. Selected parameters about the crystal structures, experiment and refinement are given in Table 1. Bond length and bond angles are summarized in Tables S1 and S2 in the Supporting Information section. C– and N–bound H atoms, for compounds **1** and **4**, were placed geometrically and refined as riding, with N–H = 0.89 Å and C–H = 0.97 Å. The H atoms of the water molecules of **1** were refined freely. For full information on the structures refinements, the reader is referred to files CIFs (for **1** CCDC 2073639, for **4** CCDC 2073638).

4.3. Hirshfeld Surface Calculation

The program CrystalExplorer [62] was used to execute Hirshfeld surface analysis to obtain additional insights concerning the crystal packing. The calculation was performed using the CIF files of the synthesized crystals. The quantification and description of the intermolecular interactions in the crystal structure are visualized using d$_{norm}$ and two-dimensional fingerprint plots. The Hirshfeld surface mapped over d$_{norm}$ takes negative or positive values depending on whether the intermolecular contact is shorter or longer, respectively, than the van der Waals radii. To visualize the intermolecular contacts on the Hirshfeld surface mapped over d$_{norm}$, a color gradient (blue-white-red) is used when the

intermolecular contacts are shorter, equal, or longer than the van der Waals separation, respectively. The two-dimensional fingerprint plot provides the decomposition of Hirshfeld surfaces into specific interatomic contacts contains information related to specific intermolecular interactions.

4.4. Catalytic Study

The compounds **2** (5–10 mol%) or **3** (5–10 mol%) and aldehyde **5** (0.1 mmol) were dissolved in the corresponding alcohol ROH **6** (0.25 mL) in a test tube (Table 5). The resulting mixture was stirred at the temperature indicated in Table 5 (40, 50, or 60 °C) for the time indicated in the same Table 5 (24, 48, or 72 h). The reactions were monitored by thin-layer chromatography. The conversions of the reaction are given by ^{1}H NMR. The final scope (Figure 9) is conducted using **3** (8 mg, 0.01 mmol) and 0.1 mmol of aldehydes **5a–i** at 60 °C and using *n*-amyl alcohol **6e** (250 μL). The reaction crudes were purified by column chromatography (neutral alumina, hexane: Et_2O, 9:0 to 9:1).

4.5. Characterization of Acetals **7ae**–**7ie**

1-(Bis(pentyloxy)methyl)-3-nitrobenzene **7ae**: compound **7ae** was obtained as a yellow oil in 92% yield. ^{1}H NMR (300 MHz, CD_3CN) δ 0.89 (t, *J* = 6.0 Hz, 6H), 1.22–1.44 (m, 8H), 1.49–1.70 (m, 4H), 3.53 (qt, *J* = 9.4, 6.5 Hz, 4H), 5.57 (s, 1H), 7.55–7.67 (m, 1H), 7.77–7.86 (m, 1H), 8.13–8.21 (m, 1H), 8.21–8.28 (m, 1H); ^{13}C-APT NMR (75 MHz, CD_3CN) δ 14.3 (2C), 23.2 (2C), 29.2 (2C), 30.1 (2C), 66.9 (2C), 101.3 (1C), 122.3 (1C), 124.1 (1C), 130.5 (1C), 134.0 (1C), 142.9 (1C), 149.3 (1C); HRMS (ESI+) calcd for $C_{17}H_{27}NNaO_4$ 332.1832, found 332.1833 [M + Na].

1-(Bis(pentyloxy)methyl)-4-nitrobenzene **7be**: compound **7be** was obtained as a yellow oil in 95% yield. ^{1}H NMR (300 MHz, CD_3CN) δ 0.80–0.98 (m, 6H), 1.22–1.43 (m, 8H), 1.47–1.68 (m, 4H), 3.52 (qt, *J* = 9.4, 6.5 Hz, 4H), 5.55 (s, 1H), 7.57–7.70 (m, 2H), 8.15–8.26 (m, 2H); ^{13}C-APT NMR (75 MHz, CD_3CN) δ 14.3 (2C), 23.2 (2C), 29.2 (2C), 30.1 (2C), 67.0 (2C), 101.5 (1C), 124.3 (2C), 128.7 (2C), 147.7 (1C), 148.9 (1C); HRMS (ESI+) calcd for $C_{17}H_{27}NNaO_4$ 332.1832, found 332.1840 [M + Na].

1-(Bis(pentyloxy)methyl)-3-chlorobenzene **7ce**: compound **7ce** was obtained as a yellow oil in 72% yield. ^{1}H NMR (300 MHz, CD_3CN) δ 0.81–0.98 (m, 6H), 1.23–1.42 (m, 8H), 1.50–1.66 (m, 4H), 3.49 (qt, *J* = 9.4, 6.5 Hz, 4H), 5.44 (s, 1H), 7.31–7.46 (m, 4H); ^{13}C-APT NMR (75 MHz, CD_3CN) δ 14.3 (2C), 23.2 (2C), 29.2 (2C), 30.1 (2C), 66.8 (2C), 101.8 (1C), 126.1 (1C), 127.5 (1C), 129.1 (1C), 130.8 (1C), 134.5 (1C), 149.1 (1C); HRMS (ESI+) calcd for $C_{17}H_{27}ClNaO_2$ 321.1592, found 321.1586 [M + Na].

1-(Bis(pentyloxy)methyl)-3-bromobenzene **7de**: compound **7de** was obtained as a yellow oil in 65% yield. ^{1}H NMR (300 MHz, CD_3CN) δ 0.73–1.05 (m, 6H), 1.17–1.46 (m, 8H), 1.46–1.70 (m, 4H), 3.49 (tdd, *J* = 15.9, 9.4, 6.6 Hz, 4H), 5.43 (s, 1H), 7.20–7.35 (m, 1H), 7.35–7.45 (m, 1H), 7.45–7.54 (m, 1H), 7.59 (s, 1H); ^{13}C-APT NMR (75 MHz, CD_3CN) δ 14.3 (2C), 23.2 (2C), 29.2 (2C), 30.1 (2C), 66.7 (2C), 101.7 (1C), 122.7 (1C), 126.5 (1C), (1C), 130.5 (1C), 131.1 (1C), 132.1 (1C), 149.3 (1C); HRMS (ESI+) calcd for $C_{17}H_{27}BrNaO_2$ 365.1087, found 365.1071 [M + Na].

1-(Bis(pentyloxy)methyl)-4-bromobenzene **7ee**: compound **7ee** was obtained as a yellow oil in 70% yield. ^{1}H NMR (300 MHz, CD_3CN) δ 0.80–0.98 (m, 6H), 1.21–1.42 (m, 8H), 1.48–1.67 (m, 4H), 3.47 (qt, *J* = 9.0, 6.0 Hz, 4H), 5.42 (s, 1H), 7.30–7.39 (m, 2H), 7.47–7.57 (m, 2H); ^{13}C-APT NMR (75 MHz, CD_3CN) δ 14.3 (2C), 23.2 (2C), 29.2 (2C), 30.2 (2C), 66.7 (2C), 102.0 (1C), 122.6 (1C), 129.6 (2C), 132.1 (2C), 140.0 (1C); HRMS (ESI+) calcd for $C_{17}H_{27}BrNaO_2$ 365.1087, found 365.1064 [M + Na].

4-(Bis(pentyloxy)methyl)benzonitrile **7fe**: compound **7fe** was obtained as a yellow oil in 95% yield. ^{1}H NMR (300 MHz, CD_3CN) δ 0.80–1.00 (m, 6H), 1.20–1.45 (m, 8H), 1.53–1.73 (m, 4H), 3.37–3.60 (m, 4H), 5.52 (s, 1H), 7.58 (d, *J* = 6.0 Hz, 2H), 7.66 (d, *J* = 9.0 Hz, 2H);

^{13}C-APT NMR (75 MHz, CD$_3$CN) δ 14.3 (2C), 23.2 (2C), 29.2 (2C), 30.1 (2C), 67.0 (2C), 101.8 (1C), 112.7 (1C), 128.5 (2C), 133.1 (2C), 145.8 (1C), 160.2 (1C); HRMS (ESI+) calcd for C$_{18}$H$_{27}$NNaO$_2$ 312.1934, found 312.1921 [M + Na].

1-(Bis(pentyloxy)methyl)-4-(trifluoromethyl)benzene **7ge**: compound **7ge** was obtained as a yellow oil in 89% yield. ^{1}H NMR (300 MHz, CD$_3$CN) δ 0.83–0.96 (m, 6H), 1.25–1.43 (m, 8H), 1.52–1.66 (m, 4H), 3.37–3.64 (m, 4H), 5.52 (s, 1H), 7.61 (d, *J* = 6.0 Hz, 2H), 7.696 (d, *J* = 9.0 Hz, 2H); ^{13}C-APT NMR (75 MHz, CD$_3$CN) δ 14.3 (2C), 23.2 (2C), 29.2 (2C), 30.2 (2C), 66.9 (2C), 101.9 (1C), 125.4 (q, *J* = 269.3 Hz, 1C), 126.0 (q, *J* = 3.8 Hz, 2C), 128.3 (2C), 130.6 (q, *J* = 55.8 Hz, 1C), 145.0 (2C); HRMS (ESI+) calcd for C$_{18}$H$_{27}$F$_3$NaO$_2$ 355.1855, found 355.1865 [M + Na].

(Bis(pentyloxy)methyl)benzene **7he:** compound **7he** was obtained as a yellow oil in 55% yield. ^{1}H NMR (300 MHz, CD$_3$CN) δ 0.74–1.05 (m, 6H), 1.18–1.43 (m, 8H), 1.50–1.66 (m, 4H), 3.34−3.63 (m, 4H), 5.44 (s, 1H), 7.25–7.53 (m, 5H); ^{13}C-APT NMR (75 MHz, CD$_3$CN) δ 14.3 (2C), 23.2 (2C), 29.2 (2C), 30.2 (2C), 66.7 (2C), 102.8 (1C), 127.5 (2C), 129.0 (2C), 129.2 (1C), 140.7 (1C); HRMS (ESI+) calcd for C$_{17}$H$_{28}$NaO$_2$ 287.1982, found 287.1968 [M + Na].

1-(Bis(pentyloxy)methyl)-4-methoxybenzene **7ie:** compound **7ie** was obtained as a yellow oil in 17% yield. ^{1}H NMR (300 MHz, CD$_3$CN) δ 0.82–0.95 (m, 6H), 1.21–1.40 (m, 8H), 1.48–1.64 (m, 4H), 3.35–3.59 (m, 4H), 3.78 (s, 3H), 5.38 (s, 1H), 6.85–6.95 (m, 2H), 7.28–7.38 (m, 2H); ^{13}C-APT NMR (75 MHz, CD$_3$CN) δ 14.3 (2C), 23.2 (2C), 29.3 (2C), 30.2 (2C), 55.9 (1C), 66.5 (2C), 102.7 (1C), 114.3 (2C), 128.8 (2C), 132.9 (1C), 160.6 (1C); HRMS (ESI+) calcd for C$_{18}$H$_{30}$NaO$_3$ 317.1787, found 317.1768 [M + Na].

5. Conclusions

In conclusion, two new organically templated perhalidometallates, (CHBMAH$_2$)ZnBr$_4$·3/2H$_2$O **1** and (CHBMAH$_2$)ZnCl$_4$ **4** have been prepared, in single-crystal form by a slow evaporation method at room temperature. A single-crystal X-ray diffraction study shows that **1** crystallizes in the non-centrosymmetric space group (P2$_1$2$_1$2), while **4** crystallizes in the centrosymmetric space groups (P2$_1$/c). The crystal packing in all obtained materials is ensured mainly by forming H-bonded networks of different dimensionality and Van der Waals interactions, which are in close agreement with the Hirshfeld surface analysis. Further, although CHBMA was utilized as a mixture of *cis* and *trans* isomers, the synthesis of **1** shows selectivity for *cis* CHBMA isomers, while other syntheses reported in the literature show selectivity for *trans* CHBMA isomers. Interestingly, the crystallization process might be a possible technique for the separation and recognition of CHBMA isomers. Finally, compound **4** was obtained during a solid-state dehydration reaction of (CHBMAH$_2$)ZnCl$_4$·2H$_2$O **2**, which took place as an uncommon single-crystal-to-single-crystal transformation. The structure of this dehydrated compound **4** contains one disordered (CHBMAH$_2$)$^{2+}$ cation with two possible cyclohexane ring positions. Such a dehydration process is associated with a change in the lattice parameters and structure reconstruction. Additionally, the catalytic activity of **2** and **3** has also been explored in the acetalization reaction of aldehydes as a model process. Both catalytic structures exhibited promising activity using different and uncommon alcohols as the unique source of acetalization. This procedure opens the door to exploring new sources of acetalization using very accessible and simple alcohols, beyond methanol or ethanol. Both parts of the catalysts (anion and cation) seem necessary to achieve such good yields. At this point, computation calculations could support a more plausible mechanism and mode of activation at molecular level.

all, (**b**) Br···H, (**c**) H···H and (**d**) O···H, Figure S2: Two-dimensional fingerprint plots with d_{norm} view of individual interaction of (CHBMAH$_2$)ZnCl$_4$, **4**: (**a**) overall, (**b**) Br···H, (**c**) H···H and (**d**) C···H, Figure S3: ^{1}H and ^{13}C-APT (CD$_3$CN) NMR spectra of 1-(bis(pentyloxy)methyl)-3-nitrobenzene **7ae**, Figure S4: ^{1}H and ^{13}C-APT (CD$_3$CN) NMR spectra of 1-(bis(pentyloxy)methyl)-4-nitrobenzene **7be**, Figure S5: ^{1}H and ^{13}C-APT (CD$_3$CN) NMR spectra of 1-(bis(pentyloxy)methyl)-3-chlorobenzene **7ce**, Figure S6: ^{1}H and ^{13}C-APT (CD$_3$CN) NMR spectra of 1-(bis(pentyloxy)methyl)-3-bromobenzene **7de**, Figure S7: ^{1}H and ^{13}C-APT (CD$_3$CN) NMR spectra of 1-(bis(pentyloxy)methyl)-4-bromobenzene **7ee**, Figure S8: ^{1}H and ^{13}C-APT (CD$_3$CN) NMR spectra of 4-(bis(pentyloxy)methyl)benzonitrile **7fe**, Figure S9: ^{1}H and ^{13}C-APT (CD$_3$CN) NMR spectra of 1-(bis(pentyloxy)methyl)-4-(trifluoromethyl) benzene **7ge**, Figure S10: ^{1}H and ^{13}C-APT (CD$_3$CN) NMR spectra of (bis(pentyloxy)methyl)benzene **7he**, Figure S11: ^{1}H and ^{13}C-APT (CD$_3$CN) NMR spectra of 1-(bis(pentyloxy)methyl)-4-methoxybenzene **7ie**.

References

1.　Luz, I.; Llabrés i Xamena, F.X.; Corma, A. Bridging homogeneous and heterogeneous catalysis with MOFs: "Click" reactions with Cu-MOF catalysts. *J. Catal.* **2010**, *276*, 134–140. [CrossRef]

2.　Zhuo, L.; Ying-Ying, L.; Guo-Hai, X.; Jian-Fang, M. Two polyoxometalate-based inorganic-organic hybrids and one coordination polymer assembled with a functionalized calix[4]arene: Catalytic and electrochemical properties. *Polyhedron* **2020**, *178*, 114324.

3.　Peipei, Z.; Ning, S.; Guodong, L.; Jing, Q.; Xiya, Y. Two Keggin polyoxometalate-based hybrid compounds with different helix: Syntheses, structure and catalytic activities. *Polyhedron* **2017**, *131*, 52–58.

4.　Rayes, A.; Herrera, R.P.; Moncer, M.; Ara, I.; Calestani, G.; Ayed, B.; Mezzadri, F. Synthesis, structural determination and catalytic study of a new 2-D chloro-substituted zinc phosphate, (C$_8$N$_2$H$_{20}$)[ZnCl(PO$_3$(OH))]$_2$. *J. Mol. Struct.* **2020**, *1202*, 127216. [CrossRef]

5.　Kagan, C.R.; Mitzi, D.B.; Dimitrakopoulos, C.D. Organic-inorganic hybrid materials as semiconducting channels in thin-film field-effect transistors. *Science* **1999**, *286*, 945–947. [CrossRef] [PubMed]

6.　Era, M.; Morimoto, S.; Tsutsui, T.; Saito, S. Organic-inorganic heterostructure electroluminescent device using a layered perovskite semiconductor (C$_6$H$_5$C$_2$H$_4$NH$_3$)$_2$PbI$_4$. *Appl. Phys. Lett.* **1994**, *65*, 676–678. [CrossRef]

7.　Joseph, A.I.; Edwards, R.L.; Luis, P.B.; Presley, S.H.; Porter, N.A.; Schneider, C. Stability and anti-inflammatory activity of the reduction-resistant curcumin analog, 2,6-dimethyl-curcumin. *Org. Biomol. Chem.* **2018**, *16*, 3273–3281. [CrossRef]

8.　Chen, J.; He, Z.-M.; Wang, F.-L.; Zhang, Z.-S.; Liu, X.-z.; Zhai, D.-D.; Chen, W.-D. Curcumin and its promise as an anticancer drug: An analysis of its anticancer and antifungal effects in cancer and associated complications from invasive fungal infections. *Eur. J. Pharmacol.* **2016**, *772*, 33–42. [CrossRef]

9.　Oladipo, S.D.; Omondi, B.; Mocktar, C. Synthesis and structural studies of nickel(II)- and copper(II)-N,N′-diarylformamidinedithiocarbamate complexes as antimicrobial and antioxidant agents. *Polyhedron* **2019**, *170*, 712–722. [CrossRef]

10.　Chung, I.; Lee, B.; He, J.; Chang, R.P.H.; Kanatzidis, M.G. All-solid-state dye-sensitized solar cells with high efficiency. *Nature* **2012**, *485*, 486–489. [CrossRef]

11.　Burschka, J.; Pellet, N.; Moon, S.-J.; Humphry-Baker, R.; Gao, P.; Nazeeruddin, M.K.; Grätzel, M. Sequential deposition as a route to high-performance perovskite-sensitized solar cells. *Nature* **2013**, *499*, 316–319. [CrossRef]

12.　Lee, M.M.; Teuscher, J.; Miyasaka, T.; Murakami, T.N.; Snaith, H.J. Efficient hybrid solar cells based on meso-superstructured organometal halide perovskites. *Science* **2012**, *338*, 643–647. [CrossRef]

13.　Liao, W.-Q.; Ye, H.-Y.; Zhang, Y.; Xiong, R.-G. Phase transitions and dielectric properties of a hexagonal ABX$_3$ perovskite-type organic–inorganic hybrid compound: [C$_3$H$_4$NS][CdBr$_3$]. *Dalton Trans.* **2015**, *44*, 10614–10620. [CrossRef]

14.　Rhouma, N.M.; Rayes, A.; Mezzadri, F.; Delmonte, D.; Cabassi, R.; Calestani, G.; Loukil, M. Structural and electrical phase transitions in the [(C$_2$H$_5$)$_4$N]$_2$ZnI$_{3.86}$Cl$_{0.14}$ system. *J. Solid State Chem.* **2017**, *256*, 60–66. [CrossRef]

15. García-Fernández, A.; Bermúdez-García, J.M.; Castro-García, S.; Llamas-Saiz, A.L.; Artiaga, R.; López-Beceiro, J.; Hu, S.; Ren, W.; Stroppa, A.; Sánchez-Andújar, M.; et al. Phase transition, dielectric properties, and ionic transport in the[(CH₃)₂NH₂]PbI₃ organic–inorganic hybrid with 2H-hexagonal perovskite structure. *Inorg. Chem.* **2017**, *56*, 4918–4927. [CrossRef]

16. Karoui, K.; Rhaiem, A.B.; Guidara, K. Dielectric properties and relaxation behavior of [TMA]₂Zn₀.₅Cu₀.₅Cl₄ compound. *Phys. B* **2012**, *407*, 489–493. [CrossRef]

17. Chen, T.; Zhou, Y.; Sun, Z.; Zhang, S.; Zhao, S.; Tang, Y.; Ji, C.; Luo, J. ABX₃-type organic–inorganic hybrid phase transition material: 1-pentyl-3-methylimidazolium tribromoplumbate. *Inorg. Chem.* **2015**, *54*, 7136–7138. [CrossRef] [PubMed]

18. Salah, A.M.B.; Fendri, L.B.; Bataille, T.; Herrera, R.P.; Naïli, H. Synthesis, structural determination and antimicrobial evaluation of two novel CoII and ZnII halogenometallates as efficient catalysts for the acetalization reaction of aldehydes. *Chem. Central J.* **2018**, *12*. [CrossRef]

19. Naïli, H.; Hajlaoui, F.; Mhiri, T.; Leod, T.C.O.M.; Kopylovich, M.N.; Mahmudov, K.T.; Pombeiro, A.J.L. 2-Dihydromethylpiperazinediium-MII (MII = CuII, FeII, CoII, ZnII) double sulfates and their catalytic activity in diastereoselectivenitroaldol (Henry) reaction. *Dalton Trans.* **2013**, *42*, 399–406. [CrossRef] [PubMed]

20. Reinoso, S.; Artetxe, B.; Gutiérrez-Zorrilla, J.M. Single-crystal-to-single-crystal transformations triggered by dehydration in polyoxometalate-based compounds. *Acta Cryst.* **2018**, *74*, 1222–1242. [CrossRef] [PubMed]

21. Wołoszyn, Ł.; Ilczyszyn, M.M.; Kinzhybalo, V. The dehydration process in the DL-phenylglycinium trifluoromethanesulfonate monohydrate crystal revealed by XRD, vibrational and DSC studies. *Acta Cryst.* **2019**, *75*, 1569–1579. [CrossRef]

22. Pasińska, K.; Piecha-Bisiorek, A.; Kinzhybalo, V.; Ciżman, A.; Gagor, A.; Pietraszko, A. A paraelectric–ferroelectric phase transition of an organically templated zinc oxalate coordination polymer. *Dalton Trans.* **2018**, *47*, 11308–11312. [CrossRef]

23. Mouchaham, G.; Roques, N.; Brandès, S.; Duhayon, C.; Sutter, J.-P. Self-assembly of Zr(C₂O₄)₄⁴⁻ metallotectons and bisimidazolium cations: Influence of the dication on H-bonded framework dimensionality and material potential porosity. *Cryst. Growth Des.* **2011**, *11*, 5424–5433. [CrossRef]

24. Emami, M.; Ślepokura, K.A.; Trzebiatowska, M.; Noshiranzadeh, N.; Kinzhybalo, V. Oxyanion clusters with antielectrostatic hydrogen bonding (AEHB) in tetraalkylammonium hypodiphosphates. *CrystEngComm* **2018**, *20*, 5209–5219. [CrossRef]

25. Rayes, A.; Moncer, M.; Ara, I.; Dege, N.; Ayed, B. Synthesis, crystal structures, Hirshfeld surface analysis and physico-chemical characterization of twonew ZnII and CdII halidometallates. *J. Mater. Sci. Mater. Electron.* **2021**, *32*, 10890–10905. [CrossRef]

26. Chihaoui, N.; Hamdi, B.; Demmak, T.; Zouari, R. Molecular structure, experimental and theoretical spectroscopic characterization and non-linear optical properties studies of a new non-centrosymmetric hybrid material. *J. Mol. Struct.* **2016**, *1123*, 144–152. [CrossRef]

27. Kubicki, M.; Szafrański, M. Hydrogen bonding in two isomorphous bis-guanidinium salts: Tetrachlorozincate(II) and tetrabromozincate(II). *J. Mol. Struct.* **1998**, *446*, 1–9. [CrossRef]

28. Chkoundali, S.; Hlel, F.; Khemekhem, H. Synthesis, crystal structure, thermal and dielectric properties of tetrapropylammonium tetrabromozincate [N(C₃H₇)₄]₂[ZnBr₄] compound. *Appl. Phys. A* **2016**, *122*, 1–8. [CrossRef]

29. Trouélan, P.; Lefebvre, J.; Derollez, P. Studies of tetramethylammonium tetrabromometallates. II. Structure of tetramethylammonium tetrabromozincate, [N(CH₃)₄]₂[ZnBr₄], in its low-temperature phase. *Acta Cryst.* **1985**, *41*, 846–850. [CrossRef]

30. Yang, L.; Powell, D.R.; Houser, R.P. Structural variation in copper (I) complexes with pyridylmethylamide ligands: Structural analysis with a new four-coordinate geometry index, τ₄. *Dalton Trans.* **2007**, 955–964. [CrossRef] [PubMed]

31. Yang, Y.; Zhao, Y.; Yu, J.; Wu, S.; Wang, R. Doping-induced structure variation of 1,3-cyclohexane−bis(methylamine)-templated zinc−phosphorus open structures. *Inorg. Chem.* **2008**, *47*, 769–771. [CrossRef]

32. Chebbi, H.; Mezrigui, S.; Jomaa, M.B.; Zid, M.F. Crystal structure, Hirshfeld surface analysis and energy framework calculation of the first oxoanion salt containing 1,3-cyclohexanebis(methylammonium): [3-(azaniumylmethyl)cyclohexyl]-methanaminiumdinitrate. *Acta Cryst.* **2018**, *74*, 949–954. [CrossRef]

33. Rhouma, N.M.; Rayes, A.; Mezzadri, F.; Calestani, G.; Loukil, M. Crystal structure of non-centrosymmetricbis(4-methoxybenzylammonium) tetrachloridozincate. *Acta Cryst.* **2016**, *72*, 1050–1053.

34. El Mrabet, R.; Kassou, S.; Tahiri, O.; Balaaraj, A.; El Ammari, L.; Saadi, M. A zero dimensional hybrid organic-inorganic perovskite ZnCl₄ based: Synthesis, crystal structure, UV-vis, and electronic properties. *J. Cryst. Growth* **2017**, *472*, 76–83. [CrossRef]

35. Leesakul, N.; Runrueng, W.; Saithong, S.; Pakawatchai, C. 2-{2-[4-(Dimethylamino)phenyl]diazen-1-ium-1-yl}pyridiniumtetrachloridozincate. *Acta Cryst.* **2012**, *68*, m837. [CrossRef]

36. El Glaoui, M.; Jeanneau, E.; Rzaigui, M.; Nars, C.B. 4-(3-Ammoniopropyl)morpholin-4-ium tetrachloridozincate(II). *Acta Cryst.* **2009**, *65*, m282. [CrossRef] [PubMed]

37. Granifo, J.; Suárez, S.; Boubeta, F.; Baggio, R. Crystallographic and computational study of a network composed of [ZnCl₄]²⁻ anions and triply protonated 4′-functionalized terpyridine cations. *Acta Cryst.* **2017**, *73*, 1121–1130. [CrossRef]

38. Perrier, P.; Byrn, S.R. Influence of crystal packing on the solid-state desolvation of purine and pyrimidine hydrates: Loss of water of crystallization from thymine monohydrate, cytosine monohydrate, 5-nitrouracil monohydrate, and S′-deoxyadenosine monohydrate. *J. Org. Chem.* **1982**, *47*, 4671–4676. [CrossRef]

39. Meskens, F.A.J. Methods for the preparation of acetals from alcohols or oxiranes and carbonyl compounds. *Synthesis* **1981**, 501–522. [CrossRef]

40. Schelhaas, M.; Waldmann, H. Protecting group strategies in organic synthesis. *Angew. Chem. Int. Ed. Engl.* **1996**, *35*, 2056–2083. [CrossRef]

41. Greene, T.W.; Wuts, P.G.M. *Protecting Groups in Organic Synthesis*, 4th ed.; Wiley-Interscience: New York, NY, USA, 2002.

42. Smirnov, A.A.; Selishcheva, S.A.; Yakovlev, V.A. Acetalization catalysts for synthesis of valuable oxygenated fuel additives from glycerol. *Catalysts* **2018**, *8*, 595. [CrossRef]

43. Karimi, B.; Golshani, B. Iodine-catalyzed, efficient and mild procedure for highly chemoselective acetalization of carbonyl compounds under neutral aprotic conditions. *Synthesis* **2002**, *33*, 784–788. [CrossRef]

44. Lee, S.H.; Lee, J.H.; Yoon, C.M. An efficient protection of carbonyls and deprotection of acetals using decaborane. *Tetrahedron Lett.* **2002**, *43*, 2699–2703. [CrossRef]

45. Leonard, N.M.; Oswald, M.C.; Freiberg, D.A.; Nattier, B.A.N.; Smith, R.C.; Mohan, R.S. A simple and versatile method for the synthesis of acetals from aldehydes and ketones using bismuth triflate. *J. Org. Chem.* **2002**, *67*, 5202–5207. [CrossRef] [PubMed]

46. Patel, S.M.; Chudasama, U.V.; Ganesphure, P.A. Ketalization of ketones with diols catalyzed by metal(IV) phosphates as solid acid catalysts. *J. Mol. Catal. A Chem.* **2003**, *194*, 267–271. [CrossRef]

47. Chen, C.-T.; Weng, S.-S.; Kao, J.-Q.; Lin, C.-C.; Jan, M.-D. Stripping off water at ambient temperature: Direct atom-efficient acetal formation between aldehydes and diols catalyzed by water-tolerant and recoverable vanadyl triflate. *Org. Lett.* **2005**, *7*, 3343–3346. [CrossRef]

48. Kumar, R.; Chakraborti, A.K. Copper(II) tetrafluoroborate as a novel and highly efficient catalyst for acetal formation. *Tetrahedron Lett.* **2005**, *46*, 8319–8323. [CrossRef]

49. Smith, B.M.; Graham, A.E. Indium triflate mediated acetalization of aldehydes and ketones. *Tetrahedron Lett.* **2006**, *47*, 9317–9319. [CrossRef]

50. Williams, D.B.G.; Lawton, M.C. Highly atom efficient aluminium triflate catalysed acetal formation. *Green Chem.* **2008**, *10*, 914–917. [CrossRef]

51. Gregg, B.T.; Golden, K.C.; Quinn, J.F. Indium(III)trifluoromethanesulfonate as a mild, efficient catalyst for the formation of acetals and ketals in the presence of acid sensitive functional groups. *Tetrahedron* **2008**, *64*, 3287–3295. [CrossRef]

52. Ono, F.; Takenaka, H.; Eguchi, Y.; Endo, M.; Sato, T. A simple and efficient procedure for the synthesis of ketone di-*sec*-alkyl acetals. *Synlett* **2009**, 487–489.

53. Miao, Z.; Xu, L.; Song, H.; Zhao, H.; Chou, L. One-pot synthesis of ordered mesoporous zirconium oxophosphate with high thermostability and acidic properties. *Catal. Sci. Technol.* **2013**, *3*, 1942–1954. [CrossRef]

54. Zhao, S.; Jia, Y.; Song, Y.-F. Acetalization of aldehydes and ketones over $H_4[SiW_{12}O_{40}]$ and $H_4[SiW_{12}O_{40}]/SiO_2$. *Catal. Sci. Technol.* **2014**, *4*, 2618–2625. [CrossRef]

55. Yi, H.; Niu, L.; Wang, S.; Liu, T.; Singh, A.K.; Lei, L. Visible-light-induced acetalization of aldehydes with alcohols. *Org. Lett.* **2017**, *19*, 122–125. [CrossRef]

56. Mensah, E.A.; Green, S.D.; West, J.; Kindoll, T.; Lazaro-Martinez, B. Formation of acetals and ketals from carbonyl compounds: A new and highly efficient method inspired by cationic palladium. *Synlett* **2019**, *30*, 1810–1814. [CrossRef]

57. Velusamy, S.; Punniyamurthy, T. Cobalt(II)-catalyzed chemoselective synthesis of acetals from aldehydes. *Tetrahedron Lett.* **2004**, *45*, 4917–4920. [CrossRef]

58. Rajabi, F. Cobalt(II) schiff base functionalized mesoporous silica as an efficient and recyclable chemoselective acetalization catalyst. *J. Iran. Chem. Soc.* **2010**, *7*, 695–701. [CrossRef]

59. Roy, A.; Rahman, M.; Das, S.; Kundu, D.; Kundu, S.K.; Majee, A.; Hajra, A. Zinc chloride as an efficient catalyst for chemoselective dimethyl acetalization. *Synth. Commun.* **2009**, *39*, 590–595. [CrossRef]

60. Saïd, S.; Naïli, H.; Bataille, T.; Herrera, R.P. Crystallisation, thermal analysis and acetal protection activity of new layered Zn(ii) hybrid polymorphs. *CrystEngComm* **2016**, *18*, 5365–5374. [CrossRef]

61. CCDC Deposition Numbers 2073639 (1), 1825834 (2), 1563308 (3) and 1548767 (4) Contain the Supplementary Crystallo-Graphic Data. These Data Can Be Obtained Free of Charge or Contacting the Cambridge Crys-Tallography Data Center (12 Union Road Cambridge CB2 1EZ United Kingdom). Available online: https://www.ccdc.cam.ac.uk/ (accessed on 22 June 2021).

62. Turner, M.J.; McKinnon, J.J.; Wolff, S.K.; Grimwood, D.J.; Spackman, P.R.; Jayatilaka, D.; Spackman, M.A. CrystalExplorer 17.5, University of Western Australia. 2007. Available online: http://hirshfeldsurface.net (accessed on 22 June 2021).